Compromised synaptic signal from prefrontal cortex to mediodorsal thalamus in Alzheimer's disease models and its rescue by kinase inhibitors

Ping Zhong, Tarek Shaker, Pei Li and Zhen Yan

Department of Physiology and Biophysics, Jacobs School of Medicine and Biomedical Sciences, State University of New York at Buffalo, Buffalo, New York, USA

Handling Editors: Katalin Toth & Samuel Young

The peer review history is available in the Supporting information section of this article (https://doi.org/10.1113/JP289018#support-information-section).

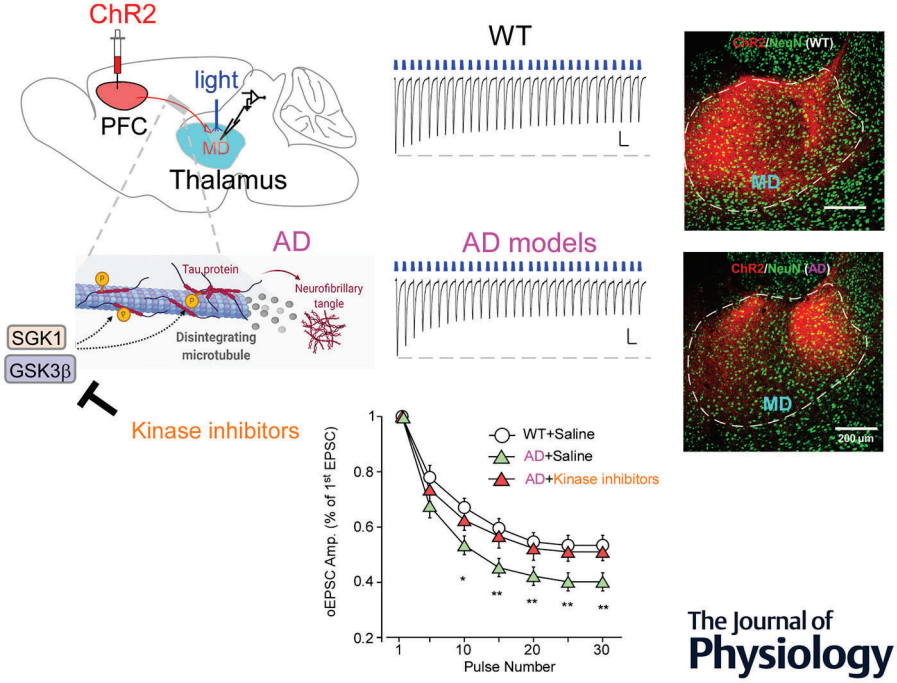

Abstract figure legend Schematic diagram showing the compromised synaptic signal from prefrontal cortex (PFC) to mediodorsal thalamus (MD) in Alzheimer's disease (AD) models and its rescue by kinase inhibitors. Optogenetic recording experiments were performed to examine the strength of PFC projections to thalamic nuclei. Two AD mouse models (P301S Tau, 5xFAD) exhibited a more significant decline in short-term depression (STD) of synaptic responses in response to repeated light stimulation of channelrhodopsin-2 (ChR2) signals in MD. Optogenetic imaging showed

Ping Zhong is currently a senior research scientist at the State University of New York at Buffalo, School of Medicine and Biomedical Sciences. He holds a PhD degree in electrical engineering from Southeast University in China. Dr Zhong has had 25 years of experience in electrophysiological techniques, especially whole-cell patch-clamp recordings of brain slices and stem cell cultures, and has published over 50 peer-reviewed articles. His research primarily focuses on the regulation of synaptic transmission in neural circuits associated with mental health and brain disorders.

DOI: 10.1113/JP289018

The Journal of Physiology

that P301S Tau mice had significantly reduced ChR2 expression in MD axon terminals innervated by PFC. Inhibiting SGK1 and GSK3β, both of which can induce tau hyperphosphorylation and the ensuing disruption of microtubule-based transport in AD, normalized STD of PFC to MD synaptic responses in Tau mice.

Abstract One of the most important neural circuits controlling cognitive processes is the projection from prefrontal cortex (PFC) to thalamus. To determine the strength of PFC projections to different thalamic nuclei, we performed optogenetic experiments by injecting channelrhodopsin-2 (ChR2) to medial PFC and recording synaptic responses evoked by light stimulation of ChR2-expressing terminals in thalamic neurons. The mediodorsal thalamus (MD) had markedly larger synaptic currents than neighbouring areas, suggesting that PFC sends prominent signals to MD. To determine whether the PFC to MD pathway is altered at early stages of Alzheimer's disease (AD), we used two mouse models (∼4 months old), transgenic mice carrying the human P301S mutation of microtubule-associated protein tau (Tau), and familial AD mice carrying five mutations on APP and PS1 (5xFAD). Both AD mouse models exhibited a more significant decline in short-term depression (STD) of synaptic responses in response to repeated light stimulation of MD ChR2 signals. Optogenetic imaging showed that Tau mice had significantly reduced ChR2 expression in MD axon terminals innervated by PFC. Next, we inhibited two kinases, serum and glucocorticoid-regulated kinase 1 (SGK1) and glycogen synthase kinase-3 beta (GSK3β), both of which can induce tau hyperphosphorylation and the ensuing disruption of microtubule-based transport in AD. Treatment with SGK1 or GSK3β inhibitor normalized STD of PFC to MD synaptic responses in Tau mice, but not in 5xFAD mice. These results suggest that the synaptic connectivity in the PFC-to-MD pathway is compromised in AD, which may be due to tau kinase-induced disruption of axonal transport.

(Received 4 April 2025; accepted after revision 27 January 2026; first published online 15 February 2026)
Corresponding author Z. Yan: State University of New York at Buffalo, 955 Main St., Buffalo, NY 14203, USA. Email: zhenyan@buffalo.edu

Key points

- Optogenetic recordings reveal the strong connection from prefrontal cortex (PFC) to mediodorsal thalamus (MD).
- Short-term depression (STD) of PFC to MD synaptic responses is altered in P301S Tau and 5xFAD mouse models of Alzheimer's disease (AD).
- Optogenetic imaging uncovers the significantly reduced PFC to MD projection in Tau mice.
- Inhibition of tau kinase SGK1 or GSK3β normalizes STD of PFC to MD synaptic responses in Tau mice, but not 5xFAD mice.
- These results suggest that the synaptic information transfer from PFC to MD pathway is compromised in AD, probably via tau kinase-induced disruption of axonal transport.

Introduction

The thalamus, which integrates signals from different sensorimotor modalities and processes the feedback signal from cortical areas, is highly implicated in cognitive functions, including learning, memory, attention and executive control (Halassa & Sherman, 2019; Li et al., 2020; Perry & Mitchell, 2019; Scott et al., 2024; Wolff & Halassa, 2024). A unique thalamic nucleus, mediodorsal thalamus (MD), has minimal connectivity with first-order sensory or motor inputs (Ouhaz et al., 2018; Parnaudeau et al., 2018), but forms reciprocal connections with prefrontal cortex (PFC) as a higher-order information processing unit (Alcaraz et al., 2016; Wolff & Halassa, 2024). While PFC holds and manipulates cognitive processing information, MD serves as a fundamental relay station of PFC (Ouhaz et al., 2018; Parnaudeau et al., 2018; Pergola et al., 2018). It transmits or amplifies the input from PFC, and provides the feedback to communicate with PFC regions (Scott et al., 2024; Wolff & Halassa, 2024). Disturbing the information flowing in the PFC–MD pathway could lead to compromised decision-making (Perry et al., 2021; Zhang et al., 2024).

Abnormal neuronal network function has been found in Alzheimer's disease (AD) (Al-Ezzi et al., 2024; Palop & Mucke, 2010), a neurodegenerative disorder characterized by cognitive impairment. Using optogenetic and electrophysiological approaches, our previous studies have revealed the alteration of specific neural circuits in aged (>6 months old) AD mouse models, including the PFC to basal forebrain (BF) cholinergic neurons (Zhong et al., 2022) and PFC to entorhinal cortex (EC) (Zhong et al., 2024). Since the identification of early signs in AD is crucial for interventions (Dubois et al., 2023; Nguyen et al., 2024), we examined circuit changes at the early stage of AD by focusing on the PFC to MD pathway in a tauopathy mouse model harbouring the human P301S mutation on the microtubule-associated protein tau (P30S Tau, 3–4 months old) and a familial AD model carrying five mutations on APP and PS1 (5xFAD, 3–4 months old).

To measure synaptic information transfer from PFC to MD, we recorded short-term depression (STD) of synaptic currents in MD neurons in response to repeated stimulation of inputs from PFC, a process serving as a low-pass filter to reduce synaptic information transfer at high presynaptic firing frequencies. The extent and kinetics of STD reflect the efficiency of synaptic information transmission that is controlled by vesicle transport and transmitter release (Schneggenburger et al., 2002; Zucker & Regehr, 2002). We found a significantly increased decline in STD of PFC to MD synaptic responses in P30S Tau and 5xFAD mice, suggesting the reduced axonal transport in this long-range pathway. Indeed, reduced axonal trafficking in PFC-to-MD connections of Tau mice measured by optogenetic imaging of PFC projections corroborates our physiological findings. Since tau hyperphosphorylation induced by various kinases plays a key role in affecting microtubule stability and axonal transport (Combs et al., 2019; Iqbal et al., 2016; Rajmohan & Reddy, 2017; Terwel et al., 2002; Wang et al., 2013), we further examined the rescuing effects on STD of inhibiting two kinases that are upregulated in AD, glucocorticoid-regulated kinase 1 (SGK1) (Cao et al., 2020; Yang et al., 2006) and glycogen synthase kinase 3 beta (GSK3β) (Hernandez et al., 2013; Sayas & Ávila, 2021; Wagner et al., 1996). The results from this study provide a potential treatment strategy for the compromised synaptic information transfer from PFC to MD at the early stage of AD.

Materials and methods

Ethical approval

All animal studies were conducted with the approval of the Institutional Animal Care and Use Committee (IACUC) at the State University of New York at Buffalo (reference number: PROTO202000049). All methods were performed in accordance with the relevant guidelines and regulations.

Animals and surgery

Wild-type (WT), Tau P301S transgenic mice (Yoshiyama et al., 2007) (Jackson Laboratory, 008169, Bar Harbor, ME, USA) and 5XFAD (Jackson Laboratory, 034848) were used in this study. Mice were kept in a temperature-controlled environment with a 12 h light/dark cycle, and had access to food and water *ad libitum*.

AAV9.CAG.hChR2(H134R)-mCherry.WPRE.SV40 (ChR2) was purchased from Addgene (#100054-AAV9, Cambridge, MA, USA; $\geq 1 \times 10^{13}$ vg/ml). Virus injection was conducted as previously described (Zhong et al., 2020, 2024). Briefly, mice (~3 months old) were anaesthetized with I.P. administration of ketamine (95 mg/kg) and xylazine (5 mg/kg). After achieving deep anaesthesia, mice were placed on top of a heating pad with their heads fixed, scalp exposed and eyes covered with ointment. Under sterile conditions, localized analgesics were applied to the head, and an incision was made. A dental drill was used to make a small opening above the injection site. Using the stereotaxic apparatus (KoPF, Tujunga, CA, USA), we injected ChR2 virus into the prelimbic cortex area (AP: 2.0 mm, ML: ±0.3 mm, DV: 2 mm) through a Hamilton syringe (34 gauge). Injection speed was controlled using a microinjection pump (KD Scientific) (100 nl/min). The injection needle was left in place for 10 min following injection then slowly withdrawn. Afterwards, the incision was resealed with sutures. The mouse was kept on a heating pad during recovery from anaesthesia before returning to the home-cage. Mice were subject to viral expression for ~4 weeks before experimentation. Both male and female mice were used for experiments and data were pooled together.

Electrophysiological and optogenetic recordings

Mice were anaesthetized via isoflurane (3–4%) inhalation and rapidly decapitated. Brains were quickly removed and submerged in ice-cold sucrose solution (in mM: 234 sucrose, 4 $MgSO_4$, 2.5 KCl, 1 NaH_2PO_4, 0.1 $CaCl_2$, 15 Hepes, 11 glucose, pH 7.35). Coronal slices (300 μm) were prepared on a vibratome (Leica VT1000s, Wetzlar, Germany) in ice-cold sucrose solution, then were transferred into artificial cerebrospinal fluid (ACSF) (in mM: 130 NaCl, 26 $NaHCO_3$, 3 KCl, 5 $MgCl_2$, 1.25 NaH_2PO_4, 1 $CaCl_2$, 10 glucose, pH 7.4, and 300 mOsm, oxygenated with 95% O_2 + 5% CO_2), and kept at ~32°C for 1 h and then at room temperature (22–24°C) for 1–4 h.

For recordings, one slice was positioned in a perfusion chamber attached to the fixed stage of an upright microscope (Olympus) and submerged in continuously flowing

oxygenated ACSF. Whole-cell patch-clamp experiments were performed with a Multiclamp 700A amplifier and Digidata 1322A data acquisition system (Molecular Devices, Sunnyvale, CA, USA). Neurons were visualized with infrared differential interference contrast video microscopy. Recording electrodes were pulled from borosilicate glass capillaries (1.5/0.86 mm OD/ID) with a micropipette puller (Sutter Instrument Co., Novato, CA, USA, model P-97). Resistance of the patch electrode was about 3 MΩ.

Optogenetic stimulation of ChR2-expressing neurons or terminals in brain slices was carried out via a microscope objective (Olympus LUMPlan FI/IR, 40× 0.80 W) using a UHP-Microscope-LED-460 system (Prizmatix) that provides >1 W collimated blue light (460 nm peak, 27 nm spectrum half width, 85% peak power at 450 nm). The blue light was triggered with TTL pulses programmed by the pClamp (Molecular Devices) data acquisition software, and an on/off precision of about 0.1 ms was determined by the software-based acquisition rate. Light pulses (duration: 5 ms) were delivered during electrophysiological recordings.

Whole-cell voltage clamp was used to measure spontaneous excitatory postsynaptic currents (sEPSCs), and optogenetically evoked EPSCs (oEPSCs) evoked by optogenetic stimulation of ChR2-expressing neurons or terminals. The internal solution contained (in mM): 130 caesium methanesulphonate, 10 CsCl, 4 NaCl, 1 $MgCl_2$, 5 EGTA, 10 Hepes, 4 Mg-ATP, 0.5 Na_2GTP and 10 sodium phosphocreatine. Whole-cell current clamp and internal solution containing (in mM: 20 KCl, 100 potassium gluconate, 10 Hepes, 4 Mg-ATP, 0.5 Na_2GTP and 10 sodium phosphocreatine) were used to measure membrane resting potential, input resistance and rheobase.

Optogenetic imaging

Four weeks after virus injection, mice were anaesthetized and transcardially perfused as previously described (Cao et al., 2020). Brain tissue was post-fixed in 4% paraformaldehyde in PBS (pH 7.4) and dehydrated with 30% sucrose in PBS for two consecutive days. Coronal sections (100 μm) were cut with a vibrating microtome (Leica VT1000 S) and stored in cryoprotectant solution at −20°C until ready to use.

For molecular marker immunolabelling, slices were first permeabilized by washing in PBST (0.3% Triton-X 100 in PBS) for 10 min at room temperature (RT), then blocked with PBST containing 3% bovine serum albumin (BSA) (1 h, RT), followed by primary antibody incubation in PBST (overnight, 4°C). The following primary antibodies were used: NeuN (1:500, Millipore, # MAB377, Billerica, MA, USA); NeuN (1:500, Cell Signaling, D4G4O, # 24307, Danvers, MA, USA); Stx1b (1:250, Proteintech, # 66437-1-Ig, Rosemont, IL, USA). The next day, slices were washed three times in PBST (10 min, RT), then incubated (3 h, RT) in the following secondary antibodies: AF488 (1:1000, ThermoFisher Scientific, # A-21202, Waltham, MA, USA); AF488 (1:1000, ThermoFisher Scientific, # A-11001); AF568 (1:1000, ThermoFisher Scientific, # A-11011), and washed three times in PBST. Finally, slices were incubated in DAPI for DNA staining (5 min, RT), mounted on slides using Prolong Diamond (ThermoFisher Scientific, P36965) and coverslipped.

Images were acquired with 10× (NA 0.4) and 63× (NA 1.4) objectives of a TCS SP8 confocal microscope (Leica) using sequential laser emission at 488, 568 and 587 nm, and the manufacturer's default detection range for AF488, AF568 and mCherry, where the same illumination setup was used for all mice. Image acquisition parameters for all objectives were set at a speed of 400 Hz unidirectional and pinhole 1 AU. Step size was 2 μm and total volume was 20 μm in all images, except for STX1/NeuN images using a 63× objective, which had 0.25 μm step size and 2.5 μm total volume. The format was 1024 × 1024 pixels for the 10× objective, and 2048 × 2048 pixels for the 63× objective. For each mouse, six slices were imaged: three slices containing the PFC between A/P +1.60 and +2.10, and three slices containing the MD between A/P −1.1 and −1.8. For each MD slice, three images were taken with the 63× objective spanning medial, central and lateral MD subdivisions (nine MD images per mouse). For determining fluorescence intensity in the MD and PFC, 63× MD images and 10× PFC images were processed through FIJI (ImageJ) using maximum intensity projection and default threshold settings. In each channel, fluorescence reading per pixel in the area of interest was corrected relative to mean fluorescent signal per pixel in background regions. For each 63× MD image, fluorescence intensity was normalized relative to the mean fluorescence intensity of all 10× PFC images from the same mouse.

Data analysis

Data were acquired (sampling rate: 10 kHz, filtering frequency: 1 kHz) using the software Clampex 9.2 (Molecular Devices). Data analyses were performed with the Clampfit software (Molecular Devices), and Mini Analysis Program (Synaptosoft, Decatur, GA, USA). Statistical analysis was performed with Prism (GraphPad, La Jolla, CA). Two-way ANOVA or two-tailed unpaired Student's *t*-test were used to determine the significance of differences between groups. All of the statistical analyses used 95% as the confidence interval. All bar graphs had mean, SEM and overlaid individual data points to

demonstrate their spread or variability. Other plots used mean and SD.

Results

Optogenetic recordings reveal the strong connection from PFC to MD

To investigate the potential alteration of PFC to thalamus pathway in AD, we first conducted optogenetic recording experiments to examine the projection of PFC to various nuclei in the thalamus. ChR2(H134R)-mCherry AAV was injected into medial PFC. oEPSCs evoked by blue light stimulation of axonal terminals in the thalamus were recorded (Fig. 1*A*). The paraventricular (PV), lateroposterior/laterodosal (LP/LD), mediodorsal (MD) and ventrolateral/posterior (VL/Po) nuclei in the thalamus (Fig. 1*B*) were selected for recordings. We found that the amplitude of oEPSCs in MD was markedly greater than that in all neighbouring areas (Fig. 1*C* and *D*, MD: 769.8 ± 29.4 pA, VL/Po: 97.2 ± 8.6 pA, LP/LD: 49.4 ± 5.2 pA, PV: 33.1 ± 7.5 pA, $n = 5$–6 cells/3 mice per group, $P = 0.0001$, one-way ANOVA). Confocal images also showed the strong axonal terminal ChR2 signals (red dots) in the thalamus, particularly in the MD region (Fig. 1*E* and *F*). These data indicate that PFC has the strongest projection to MD in the thalamus.

STD of PFC to MD synaptic responses is altered in AD mouse models

Since MD is a key node in frontal-thalamic neural circuits, integrating critical information for cognitive processing, we first examined the potential alteration of local synaptic transmission in MD neurons from two AD mouse models, the P301S Tau transgenic mice and the 5xFAD mice, at an early stage (∼4 months). Electrophysiological recordings revealed no significant changes in the amplitude or frequency of sEPSC in MD of Tau mice (Fig. 2*A* and *B*, Amplitude, WT: 12.6 ± 0.6 pA, Tau: 13.1 ± 0.6 pA, $P = 0.6$, Frequency, WT: 3.2 ± 0.4 Hz, Tau: 3.6 ± 0.4 Hz, $P = 0.5$, $n = 12$ cells/3–4 mice per group, *t*-test). Similarly, no significant changes in sEPSC were found in MD of FAD mice (Fig. 2*C* and *D*, Amplitude, WT: 13.0 ± 0.6 pA, FAD: 13.6 ± 0.8 pA, $P = 0.5$, Frequency, WT: 3.6 ± 0.5 Hz, FAD: 3.5 ± 0.5 Hz, $P = 0.9$, $n = 12$–13 cells/3–4 mice per group, *t*-test). Other membrane properties of MD neurons were also similar between WT and AD models, including membrane resting potential (Fig. 2*E*, WT: −62.9 ± 1.1 mV, Tau: −62.6 ± 1.2 mV, $P = 0.8$; WT: −63.4 ± 1.3 mV, FAD: −59.5 ± 1.6 mV, $P = 0.6$, $n = 12$–13 cells/3–4 mice per group, *t*-test), input resistance (Fig. 2*F*, WT: 203.1 ± 19.0 MΩ, Tau: 217.0 ± 17.4 MΩ, $P = 0.6$; WT: 223.2 ± 13.5 MΩ, FAD: 251.8 ± 17.2 MΩ, $P = 0.2$, $n = 11$–12 cells/3–4 mice per group, *t*-test) and Rheobase (Fig. 2*G*, WT: 31.3 ± 2.5 pA, Tau: 32.8 ± 2.6 pA, $P = 0.7$; WT: 34.4 ± 2.0 pA, FAD: 30.6 ± 2.3 pA, $P = 0.2$, $n = 8$–9 cells/3 mice per group, *t*-test).

Given the critical role of the connection between PFC and MD thalamus in executive function (Parnaudeau et al., 2018; Wolff & Halassa, 2024) that is often compromised in AD at early stages (Wu et al., 2023), we next conducted optogenetic experiments to examine the potential alteration of long-range PFC to MD projections in young AD mice (∼4 months). Repeated light pulses (10 Hz) were delivered to elicit oEPSC in MD neurons, and the amplitudes of oEPSC became smaller in response to repeated stimulations, a phenomenon called STD. We found that Tau mice showed a significantly larger decline in STD of PFC to MD synaptic responses, compared to WT mice [Fig. 3*A* and *B*, $I_{30th\ pulse}/I_{1st\ pulse}$, WT: 0.53 ± 0.03, Tau: 0.37 ± 0.03, $F_{1,16} = 7.94$, $P = 0.01$, two-way repeated-measures (rm)ANOVA]. The amplitudes of oEPSC in response to the first pulse were unchanged in Tau mice (Fig. 3*C*, WT: 559.1 ± 55.3 pA, Tau, 496.7 ± 53.8 pA, $P = 0.3$, $n = 9$ cells/3–4 mice per group, *t*-test). In 5xFAD mice, we also found a significantly larger decline in STD of PFC to MD synaptic responses (Fig. 3*D* and *E*, $I_{30th\ pulse}/I_{1st\ pulse}$, WT: 0.56 ± 0.04, FAD: 0.40 ± 0.03, $F_{1,19} = 7.45$, $P = 0.014$, two-way rmANOVA). In addition, the amplitudes of oEPSC in response to the first pulse were significantly larger in 5xFAD mice (Fig 3*F*, WT: 516.2 ± 59.8 pA, FAD, 759.3 ± 71.6 pA, $P = 0.02$, $n = 10$–11 cells/3–4 mice per group, *t*-test). Other than amplitudes, we also examined the kinetics of oEPSC in response to the 1st, 15th and 30th light stimulation. No significant differences were found on the decay time constant in Tau mice or 5XFAD mice, compared to WT mice (Fig. 3*G* and *H*, $n = 9$–11 cells/3–4 mice per group). These data suggest that synaptic information transfer from PFC to MD with repeated stimulations is compromised in both AD models.

Optogenetic imaging uncovers the significantly reduced PFC to MD projection in Tau mice

We reasoned that STD deficits could be attributed to an impaired PFC-to-MD circuit in AD. To explore this, we injected ChR2 virus (0.35 µl) into PFC, and measured the ChR2 signal transported to axon terminals at MD, including medial, central and lateral MD subdivisions, in WT and Tau mice. As shown in Fig. 4, ChR2 expression in MD was significantly reduced in Tau mice compared to WT mice (normalized ChR2 intensity in MD, all subdivisions pooled, WT: 1.09 ± 0.06, Tau: 0.82 ± 0.05, $n = 27$ images/9 slices/3 mice per group, $P = 0.0017$, *t*-test).

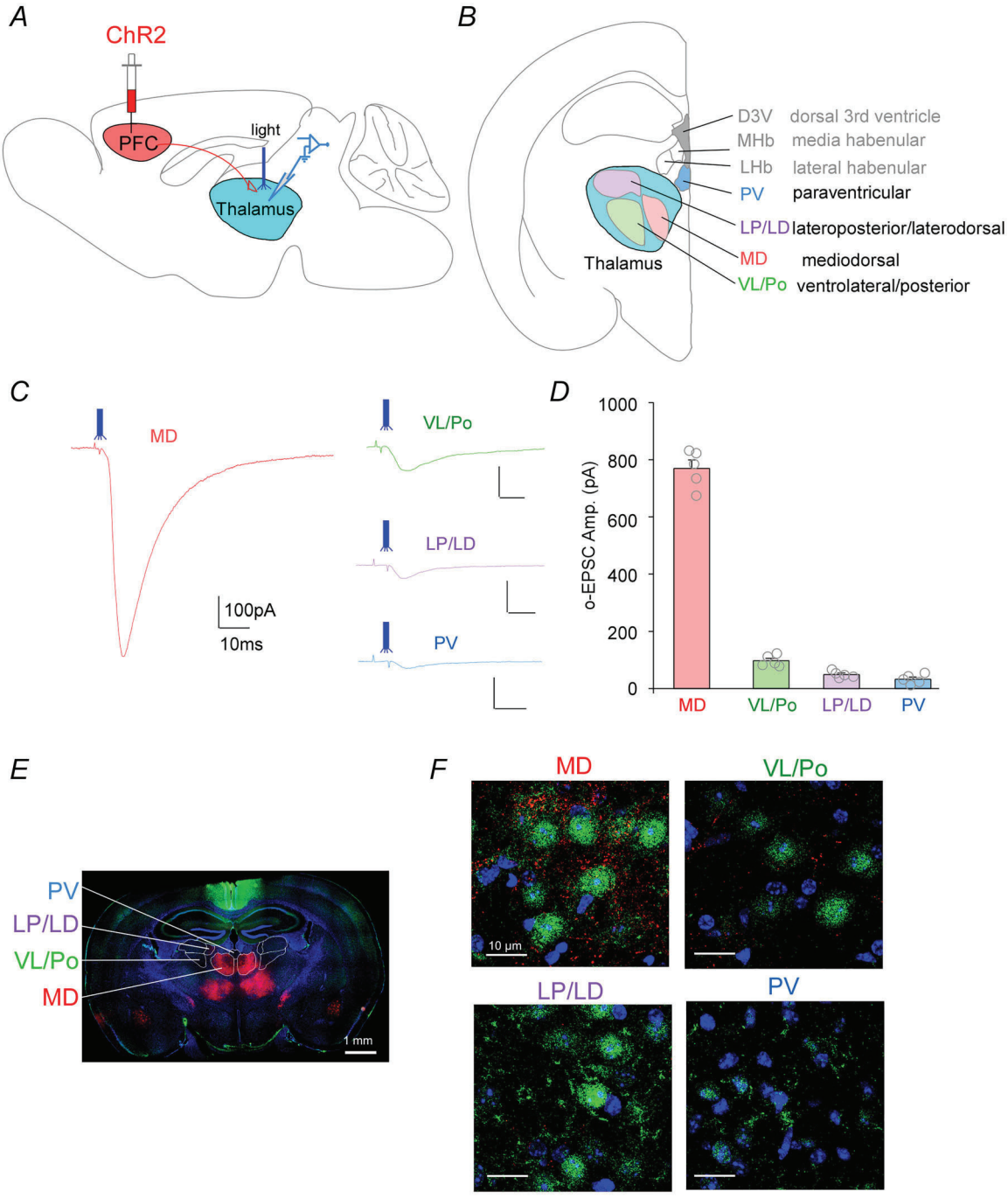

Figure 1. Optogenetic recordings reveal the functional connection from prefrontal cortex to thalamic nuclei
A, diagram showing the design of optogenetic experiments. ChR2 virus was injected to medial PFC and electrophysiological recordings were performed on thalamic neurons with blue light stimulation of ChR2-expressing terminals. *B*, diagram showing the relative location of thalamic nuclei, including paraventricular (PV), lateroposterior/laterodosal (LP/LD), mediodorsal (MD) and ventrolateral/posterior (VL/Po) regions. *C*, representative traces of EPSC evoked by optogenetic stimulation (oEPSC) in MD, VL/Po, LP/LD and PV neurons. *D*, bar graph (mean ± SEM) showing the amplitudes of oEPSC recorded in MD, LP/LD, VL/Po and PV neurons. *E*, confocal image showing Ch2R-expressing thalamic regions (red) in a mouse brain slice. *F*, high-magnification confocal images showing Ch2R-expressing terminals (red) in MD, LP/LD, VL/Po and PV regions. Cells were DAPI (blue) labelled and neurons were NeuN (green) labelled.

Staining with another synaptic marker, we also found the lower expression of Stx1b at neuronal synapses in MD of Tau mice than MD of WT mice (n = 24 images/12 slices/3 mice per group). Representative images are shown in Fig. 5. These anatomical results implicate disruption of PFC to MD axonal transport in Tau mice, which may underlie the compromised transfer of electrophysiological signals from PFC to MD.

Inhibition of SGK1 or GSK3 normalizes STD of PFC to MD synaptic responses in Tau mice, but not 5xFAD mice

Our electrophysiological and imaging data suggest reduced axonal transport in the long-range pathway. Since tau hyperphosphorylation induced by various kinases plays a key role in affecting microtubule stability and axonal transport (Turab Naqvi et al., 2020), we next

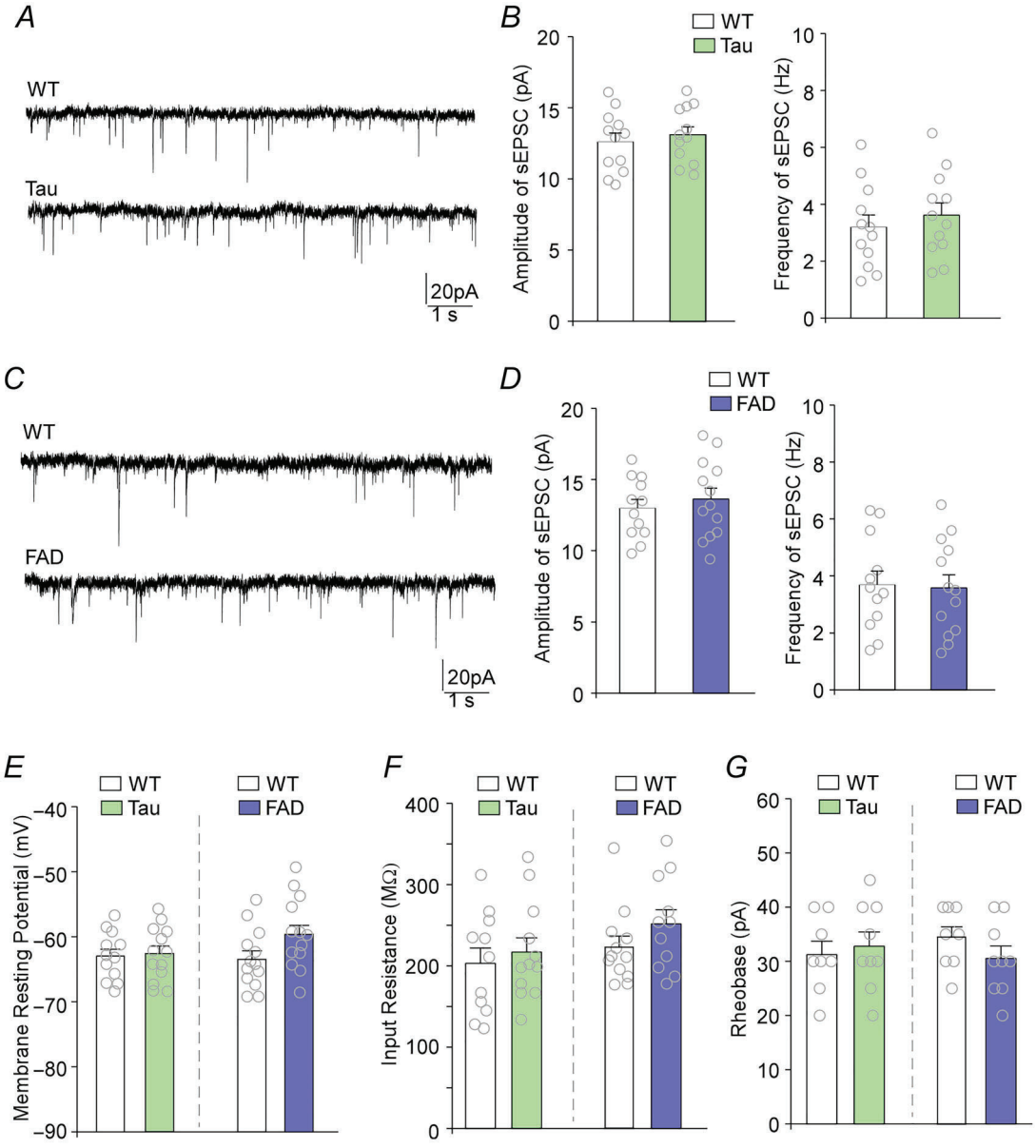

Figure 2. MD thalamic synaptic transmission and neuronal membrane properties are intact in two AD mouse models
A and *C*, representative sEPSC traces in MD neurons from WT *vs*. Tau mice (*A*) or 5xFAD mice (*C*). *B* and *D*, bar graphs (mean ± SEM) showing the amplitudes and frequencies of sEPSC in MD neurons from WT *vs*. Tau mice (*B*) or 5xFAD mice (*D*). *E*–*G*, bar graphs (mean ± SEM) showing resting membrane potential (*E*), input resistance (*F*) and Rheobase (*G*) in MD neurons from WT *vs*. Tau mice or 5xFAD mice,

examined the possibility of inhibiting tau kinases in rescuing synaptic information transfer from PFC to MD.

One of the upregulated kinases that can lead to tau hyperphosphorylation in AD is SGK1 (Cao et al., 2020; Yang et al., 2006). To determine the impact of SGK1 inhibition on STD of PFC to MD synaptic responses in Tau mice, we gave animals I.P. injections of the SGK1 inhibitor GSK650394 (1 mg/kg, I.P., once daily for 3 days) (Cao et al., 2020). We found that SGK1 inhibitor-treated Tau mice had significantly less decline in STD of PFC to MD synaptic responses, compared to saline-treated Tau mice (Fig. 6*A* and *B*, $I_{30th\ pulse}/I_{1st\ pulse}$, Tau+sal.:

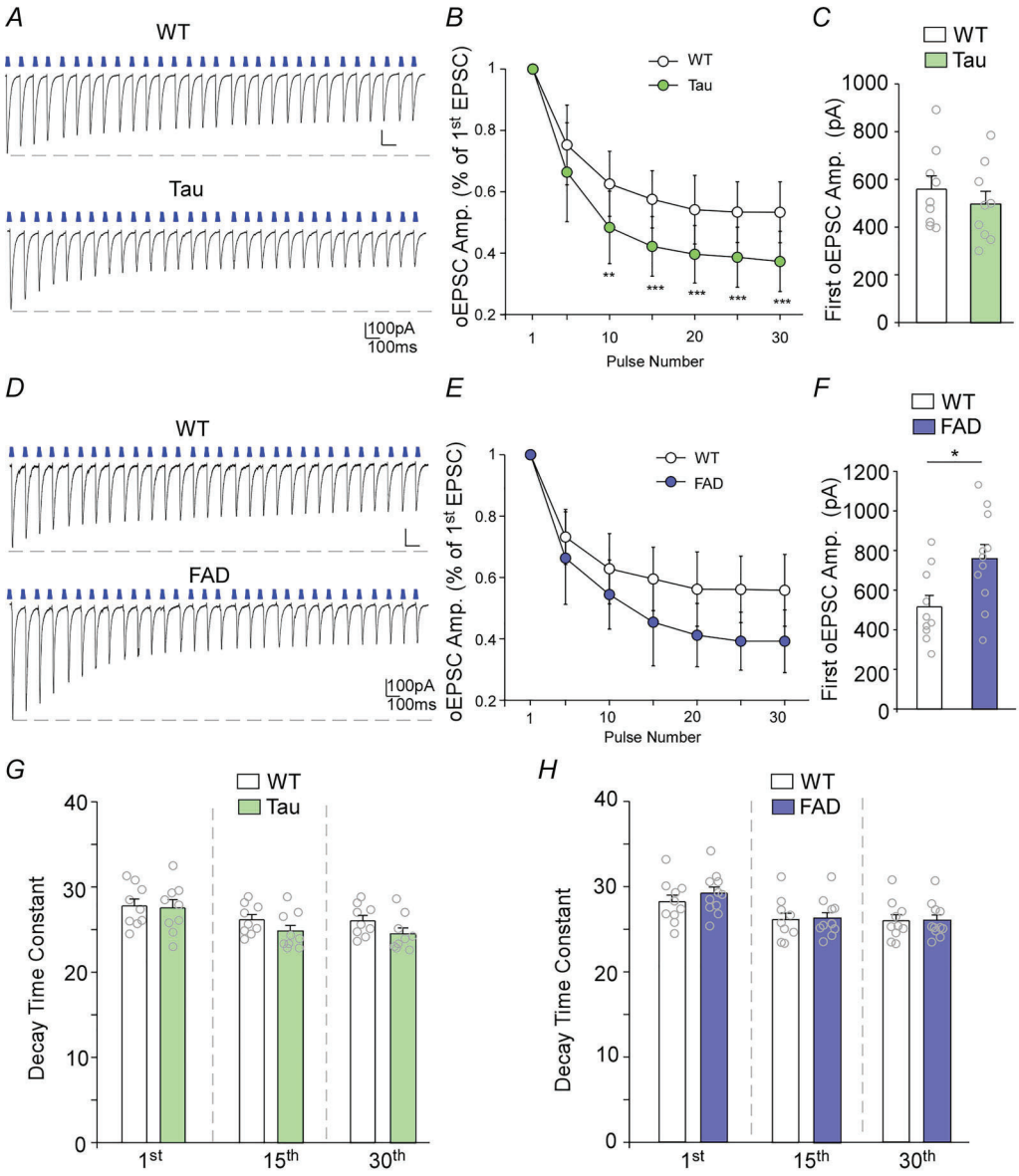

Figure 3. Short-term depression (STD) of PFC to MD synaptic responses is altered in two AD mouse models.
A and *D*, representative traces of oEPSC evoked by a train of light pulses (10 Hz) in MD neurons from WT *vs*. Tau mice (*A*) or 5xFAD mice (*D*). *B* and *E*, plots (mean ± SD) showing the depression of oEPSC amplitude (percentage of the 1st oEPSC) in response to repeated stimulation pulses in MD neurons from WT *vs*. Tau mice (*B*) or 5xFAD mice (*E*). $^{*}P < 0.05$, $^{**}P < 0.01$, $^{***}P < 0.001$, two-way rmANOVA. *C* and *F*, bar graphs (mean ± SEM) showing the amplitude of oEPSC in response to the 1st pulse in MD neurons from WT *vs*. Tau mice (*C*) or 5xFAD mice (*F*). $^{*}P < 0.05$, *t*-test. *G* and *H*, bar graphs (mean ± SEM) showing the exponential decay time constant at the 1st, 15th and 30th oEPSC in MD neurons from WT *vs*. Tau mice (*G*) or WT *vs*. 5xFAD mice (*H*).

0.40 ± 0.03, Tau+SGK1i: 0.51 ± 0.03, $F_{3,34(\text{genotype})} = 5.34$, $P = 0.0038$, *post hoc*: $P = 0.04$, Tau+sal. *vs.* Tau+SGK1i, $n = 9$–10 cells/3 mice per group, two-way rmANOVA). The amplitudes of the oEPSC in response to the first pulse were not significantly altered by GSK650394 treatment in WT or Tau mice (Fig. 6*C*, $F_{1,34(\text{genotype})} = 2.85$, $P = 0.08$, $F_{1,34(\text{treatment})} = 1.21$, $P = 0.3$, two-way ANOVA).

Another kinase that plays a key role in increasing tau phosphorylation and microtubule rearrangement in AD is GSK3β (Hernandez et al., 2013; Wagner

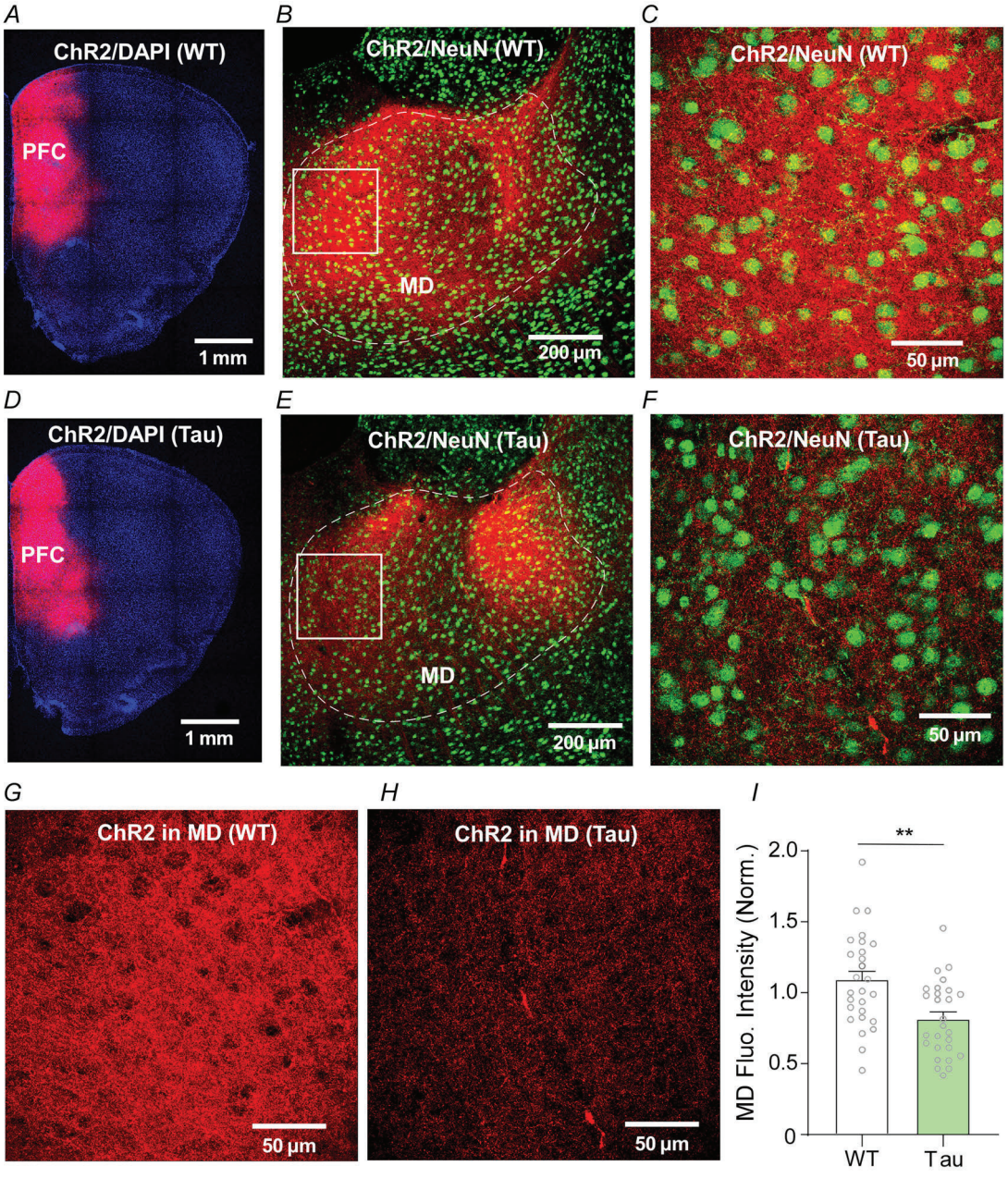

Figure 4. Optogenetic imaging reveals the reduced PFC to MD thalamic projection in Tau mice
A and *D*, representative images of mCherry-tagged ChR2 (red) virus expression in the PFC of WT (*A*) and Tau (*D*) mice. *B* and *E*, representative images of ChR2 expression (red) and NeuN neuronal marker (green) in the MD of WT (*B*) and Tau (*E*) mice following virus injection to PFC. *C* and *F*, enlarged images of *B* and *E* in the boxed area with merged ChR2 and NeuN. *G* and *H*, images of *C* and *F* with ChR2 channel only. *I*, bar graphs (mean ± SEM) showing normalized fluorescence intensity of ChR2 in MD of WT *vs.* Tau mice. $^{**}P < 0.01$, *t*-test.

et al., 1996). Lithium is known to inhibit GSK3β activity (Chalecka-Franaszek & Chuang, 1999; Ryves & Harwood, 2001), so we gave Tau mice a LiCl treatment (100 mg/kg, I.P., twice daily for 5 days) (Noble et al., 2005; Wang et al., 2020) and tested the impact of GSK3β inhibition on STD of PFC to MD synaptic responses. We found that GSK3β inhibitor-treated Tau mice also showed significantly less decline in STD of PFC to MD synaptic responses, compared to saline-treated Tau mice (Fig. 7*A* and *B*, $I_{30th\ pulse}/I_{1st\ pulse}$, Tau+sal.: 0.43 ± 0.03, Tau+GSK3i: 0.55 ± 0.03, $F_{3,40(genotype)} = 4.26$, $P = 0.01$, *post hoc*: $P = 0.017$, Tau+sal. *vs.* Tau+GSK3i, $n = 10$–12 cells/3–4 mice per group, two-way rmANOVA). The amplitudes of the oEPSC in response to the first pulse were not significantly altered by LiCl treatment in WT or Tau mice (Fig. 7*C*, $F_{1,40(genotype)} = 3.34$, $P = 0.07$, $F_{1,40(treatment)} = 0.22$, $P = 0.9$, two-way ANOVA).

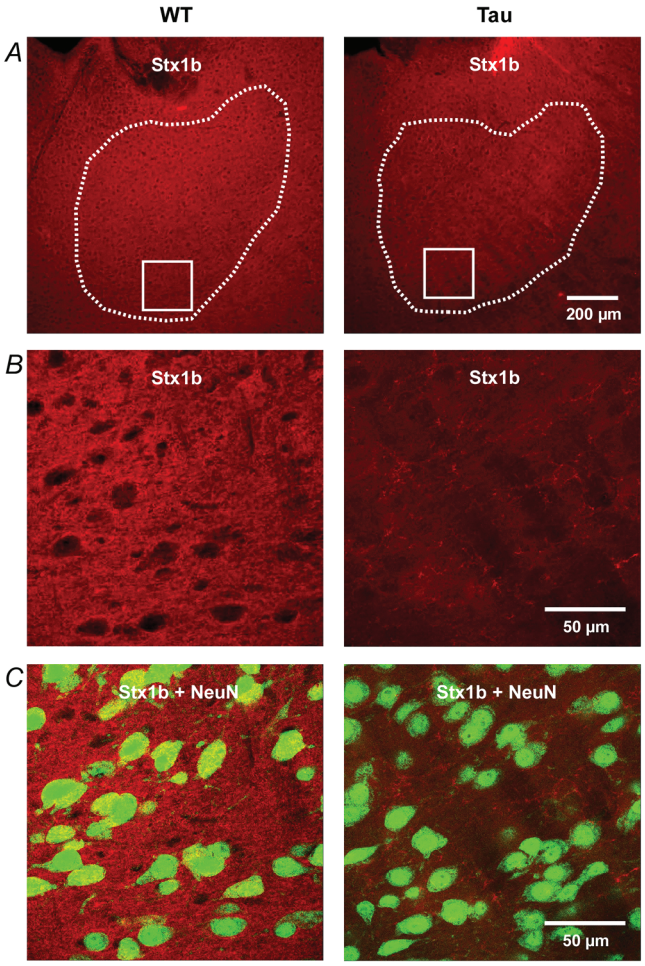

Figure 5. Immunostaining reveals the reduced synaptic marker Stx1b in Tau mice
A, representative images of Stx1b expression (red) in the MD of WT and Tau mice. *B* and *C*, enlarged images of *A* in the boxed area with Stx1b (red) only (*B*) or merged Stx1b (red) and NeuN (green) (*C*) in the MD of WT and Tau mice.

We next performed similar experiments in 5xFAD mice. We found that the SGK1 inhibitor GSK650394 failed to normalize the decline in STD of PFC to MD synaptic responses in 5xFAD mice (Fig. 8*A* and *B*, $I_{30th\ pulse}/I_{1st\ pulse}$, FAD+saline: 0.46 ± 0.03, FAD+SGK1i: 0.48 ± 0.03, $F_{3,42(genotype)} = 3.35$, $P = 0.03$, *post hoc*: $P = 0.927$, FAD+sal. *vs.* FAD+SGK1i, $n = 11$–12 cells/3–4 mice per group, two-way rmANOVA). The significantly increased amplitudes of oEPSC in response to the first pulse in 5xFAD mice were unaffected by SGK1 inhibition (Fig. 8*C*, $F_{1,42(genotype)} = 13.1$, $P = 0.0011$, $F_{1,42(treatment)} = 0.24$, $P = 0.6$, *post hoc:* $P = 0.03$, WT+sal. *vs.* FAD+sal.; $P = 0.03$, WT+SGK1i *vs.* FAD+SGK1i, two-way ANOVA). In addition, the GSK3β inhibitor LiCl also failed to normalize the decline in STD of PFC to MD synaptic responses (Fig. 8*D* and *E*, $I_{30th\ pulse}/I_{1st\ pulse}$, FAD+sal.: 0.44 ± 0.03, FAD+GSK3i: 0.47 ± 0.03, $F_{3,43(genotype)} = 2.86$, $P = 0.04$, *post hoc*: $P = 0.9$, FAD+sal. *vs.* FAD+GSK3i, $n = 10$–13 cells/3–4 mice per group, two-way rmANOVA) or change the increased amplitudes of oEPSC in response to the first pulse in 5xFAD mice (Fig. 8*F*, $F_{1,43(genotype)} = 18.7$, $P = 0.0001$, $F_{1,43(treatment)} = 0.013$, $P = 0.9$, *post hoc*: $P = 0.009$, WT+sal. *vs.* FAD+sal., $P = 0.8$, FAD+sal. *vs.* FAD+GSK3i, two-way ANOVA).

Discussion

In this study, we first used optogenetic and electrophysiological approaches to reveal the functional connectivity between PFC and thalamus. We found that the MD, a perceived executive structure in working memory processing (Bolkan et al., 2017; Wolff & Halassa, 2024), is the primary target of PFC projections (Fig. 1). In comparing with our previous measurements of opto-EPSC in PFC target regions, including BF, EC, striatum and basolateral amygdala (BLA) (Wang et al., 2022; Zhong et al., 2022, 2024), we found that opto-EPSC in MD had significantly larger amplitudes, suggesting that PFC forms a prominent synaptic connection with MD. This is corroborated by the imaging data showing that MD is enriched in ChR2-positive signals originated from PFC. Consistently, MD is considered an essential partner of PFC for higher-order cognitive function, serving the critical role of amplifying and sustaining cortical representations to guide behaviours (Parnaudeau et al., 2018).

With MD as a potential therapeutic target for improving cognitive deficits in brain disorders (Parnaudeau et al., 2018; Perry et al., 2021), we examined the functional alteration of MD neurons in AD. No significant change was found on basal synaptic transmission in local MD circuits of two AD mouse models, P301S Tau and 5xFAD, at the early stage (Fig. 2). We then examined

the potential alteration of the long-range PFC to MD functional circuit in AD. To reflect the efficiency of vesicle transport and transmitter release in the PFC→MD pathway, we measured STD, a form of synaptic plasticity characterized by the progressively decreased postsynaptic responses after repetitive stimulations of presynaptic neurons at high frequencies. We found a significantly greater decline in STD of opto-EPSC in P301S Tau and 5xFAD mice (Fig. 3), suggesting that synaptic information transfer from PFC to MD is compromised in AD. The greater current in initial pulse in 5xFAD mice (Fig. 3F) could drive greater depletion of vesicles. In accordance with these functional results, reduction of PFC-to-MD axonal transport manifested by Tau mice (Fig. 4) provides further evidence that Tau accumulation impinges deleterious effects on synaptic transmission within PFC→MD networks. Given the critical role of the PFC→MD pathway in cognition, this circuit aberration may contribute to mild cognitive impairment at the early stage of AD.

One of the primary factors that could lead to the disruption of microtubule-based transport of important cargos along axons is the hyperphosphorylation and aggregation of tau protein (Iqbal et al., 2016; Terwel et al., 2002; Wang et al., 2013). Targeting tau hyperphosphorylation via kinase inhibition has been suggested as a strategy for AD treatment (Basheer et al., 2023; Turab Naqvi et al., 2020; Xia et al., 2021). We found that

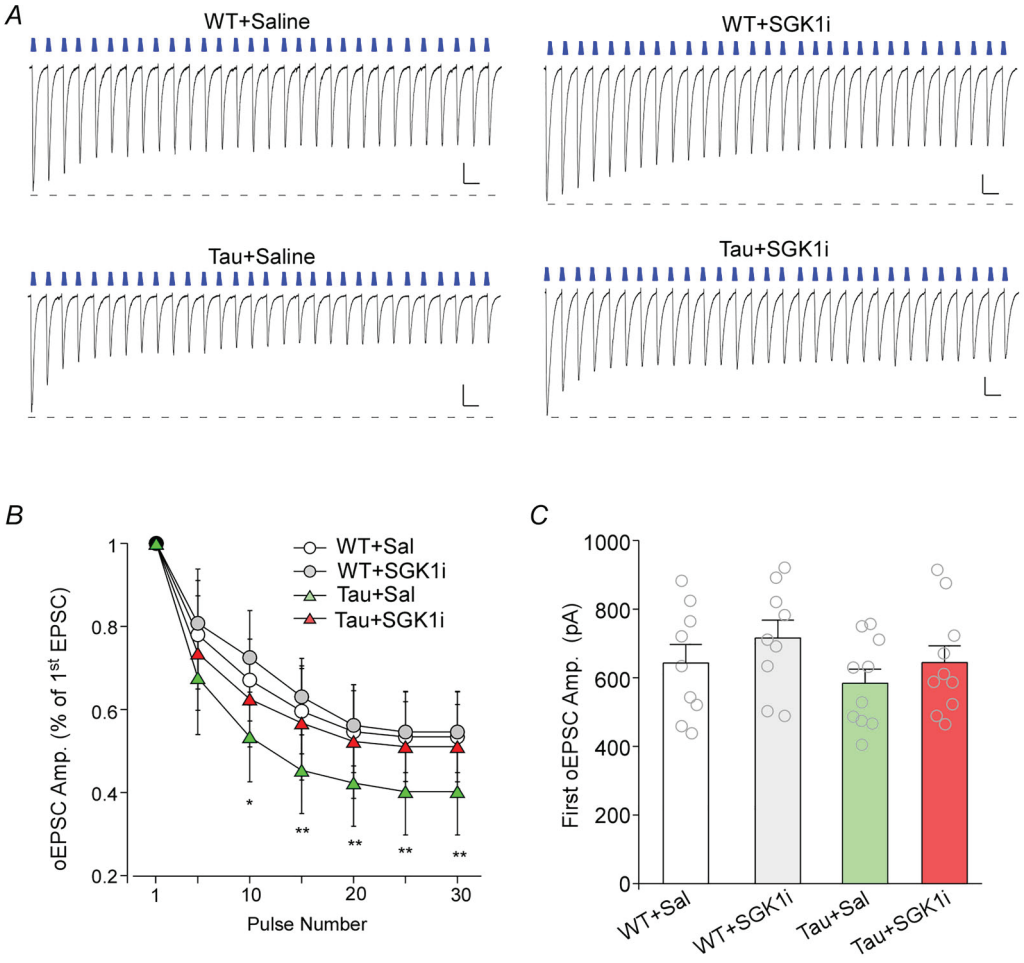

Figure 6. SGK1 inhibitor normalizes STD of PFC to MD synaptic responses in Tau mice
A, representative traces of oEPSC evoked by a train of light pulses (10 Hz) in MD neurons from WT *vs*. Tau mice treated with saline *vs*. SGK1 inhibitor GSK650394 (1 mg/kg, I.P., once daily for 3 days). *B*, plots (mean ± SD) showing the depression of oEPSC amplitude (percentage of the 1st oEPSC) in response to repeated stimulation pulses in MD neurons from WT *vs*. Tau mice treated with saline *vs*. SGK1 inhibitor. $^{*}P < 0.05$, $^{**}P < 0.01$, two-way rmANOVA. *C*, bar graphs (mean ± SEM) showing the amplitude of oEPSC in response to the 1st pulse in MD neurons from WT *vs*. Tau mice treated with saline *vs*. SGK1 inhibitor.

inhibiting two tau kinases, SGK1 or GSK3β, prevented the excessive decline in STD of PFC to MD synaptic responses in P301S Tau mice (Figs 6 and 7), suggesting that SGK1 and GSK3β could be molecular targets for restoring synaptic information transfer in neural circuits of AD brains. In agreement with this, our previous studies have found that treatment of Tau mice with the SGK1 inhibitor GSK650394 reduces tau phosphorylation and ameliorates cognitive deficits (Cao et al., 2020). Inhibition of GSK3β by lithium has also been found to correlate with reduced tauopathy and degeneration *in vivo* (Noble et al., 2005). As STD is determined by transmitter release that relies on axonal trafficking, our data on the restoration of STD by inhibiting these kinases in Tau mice suggest that the rescue effects are probably due to the restoration of axonal trafficking.

In contrast to what was found in Tau mice, SGK1 or GSK3β inhibitors failed to normalize STD in 5xFAD mice (Fig. 8). This suggests that the compromised PFC to MD circuits in 5xFAD mice may be mainly caused by Aβ-induced disruption of axonal transport, which cannot be ameliorated by targeting tau kinases. Furthermore, the Aβ–tau interaction is found to accelerate cognitive decline (Busche & Hyman, 2020; Sperling et al., 2019). Thus, new interventions are needed to restore PFC–MD circuits in AD with both Aβ and tau pathologies.

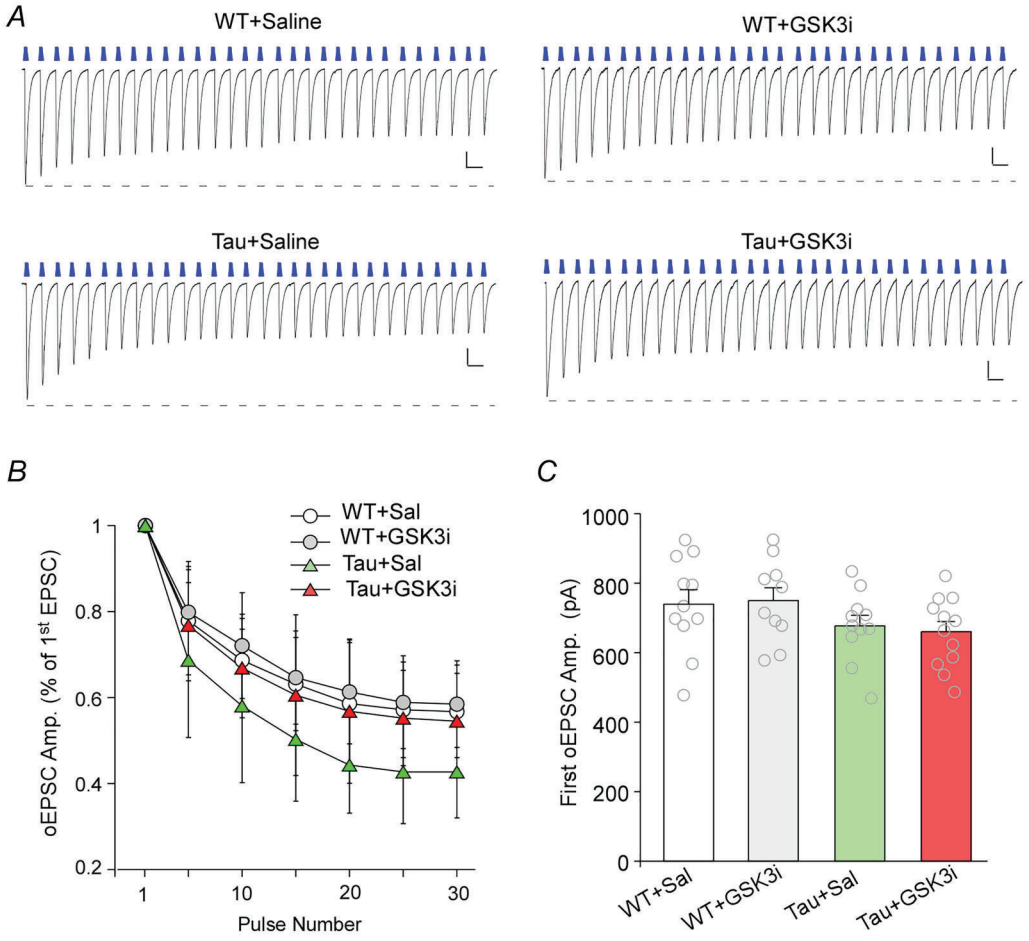

Figure 7. GSK3β inhibitor restores STD of PFC to MD synaptic responses in Tau mice
A, representative traces of oEPSC evoked by a train of light pulses (10 Hz) in MD neurons from WT *vs*. Tau mice treated with saline *vs*. GSK3β inhibitor LiCl (100 mg/kg, I.P., twice daily for 5 days). *B*, plots (mean ± SD) showing the depression of oEPSC amplitude (percentage of the 1st oEPSC) in response to repeated stimulation pulses in MD neurons from WT *vs*. Tau mice treated with saline *vs*. GSK3β inhibitor. $^{*}P < 0.05$, $^{**}P < 0.01$, two-way rmANOVA. *C*, bar graphs (mean ± SEM) showing the amplitude of oEPSC in response to the 1st pulse in MD neurons from WT *vs*. Tau mice treated with saline *vs*. GSK3β inhibitor.

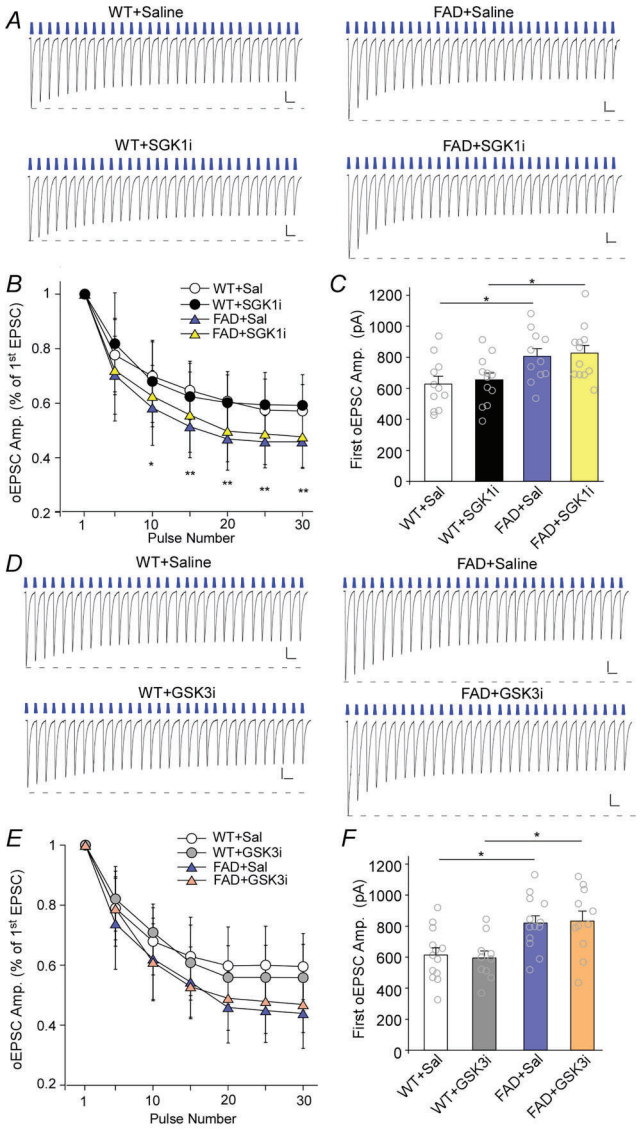

Figure 8. SGK1 or GSK3β inhibitor has no effect on the altered STD of PFC to MD synaptic responses in 5xFAD mice
A and *D*, representative traces of oEPSC evoked by a train of light pulses (10 Hz) in MD neurons from WT *vs*. 5xFAD mice treated with saline *vs*. SGK1 inhibitor GSK650394 (*A*) or GSK3β inhibitor LiCl (*D*). *B* and *E*, plots (mean ± SD) showing the depression of oEPSC amplitude (percentage of the 1st oEPSC) in response to repeated stimulation pulses in MD neurons from WT *vs*. 5xFAD mice treated with saline *vs*. SGK1 inhibitor (*B*) or GSK3β inhibitor (*E*).*$P < 0.05$, **$P < 0.01$, ***$P < 0.001$, two-way rmANOVA. *C* and *F*, bar graphs (mean ± SEM) showing the amplitude of oEPSC in response to the 1st pulse in MD neurons from WT *vs*. 5xFAD mice treated with saline *vs*. SGK1 inhibitor (*C*) or GSK3β inhibitor (*F*).

References

Al-Ezzi, A., Arechavala, R. J., Butler, R., Nolty, A., Kang, J. J., Shimojo, S., Wu, D. A., Fonteh, A. N., Kleinman, M. T., Kloner, R. A., & Arakaki, X. (2024). Disrupted brain functional connectivity as early signature in cognitively healthy individuals with pathological CSF amyloid/tau. *Communications Biology*, **7**, 1037.

Alcaraz, F., Marchand, A. R., Courtand, G., Coutureau, E., & Wolff, M. (2016). Parallel inputs from the mediodorsal thalamus to the prefrontal cortex in the rat. *European Journal of Neuroscience*, **44**(3), 1972–1986.

Basheer, N., Smolek, T., Hassan, I., Liu, F., Iqbal, K., Zilka, N., & Novak, P. (2023). Does modulation of tau hyperphosphorylation represent a reasonable therapeutic strategy for Alzheimer's disease? From preclinical studies to the clinical trials. *Molecular Psychiatry*, **28**(6), 2197–2214.

Bolkan, S. S., Stujenske, J. M., Parnaudeau, S., Spellman, T. J., Rauffenbart, C., Abbas, A. I., Harris, A. Z., Gordon, J. A., & Kellendonk, C. (2017). Thalamic projections sustain prefrontal activity during working memory maintenance. *Nature Neuroscience*, **20**(7), 987–996.

Busche, M. A., & Hyman, B. T. (2020). Synergy between amyloid-β and tau in Alzheimer's disease. *Nature Neuroscience*, **23**(10), 1183–1193.

Cao, Q., Wang, W., Williams, J. B., Yang, F., Wang, Z. J., & Yan, Z. (2020). Targeting histone K4 trimethylation for treatment of cognitive and synaptic deficits in mouse models of Alzheimer's disease. *Science Advances*, **6**(50), eabc8096

Chalecka-Franaszek, E., & Chuang, D. M. (1999). Lithium activates the serine/threonine kinase Akt-1 and suppresses glutamate-induced inhibition of akt-1 activity in neurons. *Proceedings of the National Academy of Sciences*, **96**(15), 8745–8750.

Combs, B., Mueller, R. L., Morfini, G., Brady, S. T., & Kanaan, N. M. (2019). Tau and axonal transport misregulation in tauopathies. *Advances in Experimental Medicine and Biology*, **1184**, 81–95.

Dubois, B., von Arnim, C. A. F., Burnie, N., Bozeat, S., & Cummings, J. (2023). Biomarkers in Alzheimer's disease: Role in early and differential diagnosis and recognition of atypical variants. *Alzheimer's Research & Therapy*, **15**(1), 175.

Halassa, M. M., & Sherman, S. M. (2019). Thalamocortical circuit motifs: A general framework. *Neuron*, **103**(5), 762–770.

Hernandez, F., Lucas, J. J., & Avila, J. (2013). GSK3 and tau: Two convergence points in Alzheimer's disease. *Journal of Alzheimer's Disease*, **33**(1), S141–S144.

Iqbal, K., Liu, F., & Gong, C. X. (2016). Tau and neurodegenerative disease: The story so far. *Nature Reviews Neurology*, **12**(1), 15–27.

Li, Y., Lopez-Huerta, V. G., Adiconis, X., Levandowski, K., Choi, S., Simmons, S. K., Arias-Garcia, M. A., Guo, B., Yao, A. Y., Blosser, T. R., Wimmer, R. D., Aida, T., Atamian, A., Naik, T., Sun, X., Bi, D., Malhotra, D., Hession, C. C., Shema, R., Gomes, M., … Feng, G. (2020). Distinct subnetworks of the thalamic reticular nucleus. *Nature*, **583**(7818), 819–824.

Nguyen, H. V., Mital, S., Knopman, D. S., & Alexander, G. C. (2024). Cost-effectiveness of lecanemab for individuals with early-stage Alzheimer disease. *Neurology*, **102**(7), e209218.

Noble, W., Planel, E., Zehr, C., Olm, V., Meyerson, J., Suleman, F., Gaynor, K., Wang, L., LaFrancois, J., Feinstein, B., Burns, M., Krishnamurthy, P., Wen, Y., Bhat, R., Lewis, J., Dickson, D., & Duff, K. (2005). Inhibition of glycogen synthase kinase-3 by lithium correlates with reduced tauopathy and degeneration in vivo. *Proceedings of the National Academy of Sciences*, **102**(19), 6990–6995.

Ouhaz, Z., Fleming, H., & Mitchell, A. S. (2018). Cognitive functions and neurodevelopmental disorders involving the prefrontal cortex and mediodorsal thalamus. *Frontiers in Neuroscience*, **12**, 33.

Palop, J. J., & Mucke, L. (2010). Amyloid-beta-induced neuronal dysfunction in Alzheimer's disease: From synapses toward neural networks. *Nature Neuroscience*, **13**(7), 812–818.

Parnaudeau, S., Bolkan, S. S., & Kellendonk, C. (2018). The mediodorsal thalamus: An essential partner of the prefrontal cortex for cognition. *Biological Psychiatry*, **83**(8), 648–656.

Pergola, G., Danet, L., Pitel, A. L., Carlesimo, G. A., Segobin, S., Pariente, J., Suchan, B., Mitchell, A. S., & Barbeau, E. J. (2018). The regulatory role of the human mediodorsal thalamus. *Trends in Cognitive Sciences*, **22**(11), 1011–1025.

Perry, B. A. L., Lomi, E., & Mitchell, A. S. (2021). Thalamocortical interactions in cognition and disease: The mediodorsal and anterior thalamic nuclei. *Neuroscience and Biobehavioral Reviews*, **130**, 162–177.

Perry, B. A. L., & Mitchell, A. S. (2019). Considering the evidence for anterior and laterodorsal thalamic nuclei as higher order relays to cortex. *Frontiers in Molecular Neuroscience*, **12**, 167.

Rajmohan, R., & Reddy, P. H. (2017). Amyloid-beta and phosphorylated tau accumulations cause abnormalities at synapses of Alzheimer's disease neurons. *Journal of Alzheimer's Disease*, **57**(4), 975–999.

Ryves, W. J., & Harwood, A. J. (2001). Lithium inhibits glycogen synthase kinase-3 by competition for magnesium. *Biochemical and Biophysical Research Communications*, **280**(3), 720–725.

Sayas, C. L., & Ávila, J. (2021). GSK-3 and tau: A key duet in Alzheimer's disease. *Cells*, **10**(4), 721.

Schneggenburger, R., Sakaba, T., & Neher, E. (2002). Vesicle pools and short-term synaptic depression: Lessons from a large synapse. *Trends in Neuroscience (Tins)*, **25**(4), 206–212.

Scott, D. N., Mukherjee, A., Nassar, M. R., & Halassa, M. M. (2024). Thalamocortical architectures for flexible cognition and efficient learning. *Trends in Cognitive Sciences*, **28**(8), 739–756.

Sperling, R. A., Mormino, E. C., Schultz, A. P., Betensky, R. A., Papp, K. V., Amariglio, R. E., Hanseeuw, B. J., Buckley, R., Chhatwal, J., Hedden, T., Marshall, G. A., Quiroz, Y. T., Donovan, N. J., Jackson, J., Gatchel, J. R., Rabin, J. S., Jacobs, H., Yang, H. S., Properzi, M., … Johnson, K. A. (2019). The impact of amyloid-beta and tau on prospective cognitive decline in older individuals. *Annals of Neurology*, **85**(2), 181–193.

Terwel, D., Dewachter, I., & Van Leuven, F. (2002). Axonal transport, tau protein, and neurodegeneration in Alzheimer's disease. *Neuromolecular Medicine*, **2**(2), 151–166.

Turab Naqvi, A. A., Hasan, G. M., & Hassan, M. I. (2020). Targeting tau hyperphosphorylation via kinase inhibition: Strategy to address Alzheimer's disease. *Current Topics in Medicinal Chemistry*, **20**(12), 1059–1073.

Wagner, U., Utton, M., Gallo, J. M., & Miller, C. C. (1996). Cellular phosphorylation of tau by GSK-3 beta influences tau binding to microtubules and microtubule organisation. *Journal of Cell Science*, **109**(6), 1537–1543.

Wang, J. Z., Xia, Y. Y., Grundke-Iqbal, I., & Iqbal, K. (2013). Abnormal hyperphosphorylation of tau: Sites, regulation, and molecular mechanism of neurofibrillary degeneration. *Journal of Alzheimer's Disease*, **33**(1), S123–S139.

Wang, Y., An, X., Zhang, X., Liu, J., Wang, J., & Yang, Z. (2020). Lithium chloride ameliorates cognition dysfunction induced by sevoflurane anesthesia in rats. *Federation of European Biochemical Societies Open Biology*, **10**(2), 251–258.

Wang, Z. J., Shwani, T., Liu, J., Zhong, P., Yang, F., Schatz, K., Zhang, F., Pralle, A., & Yan, Z. (2022). Molecular and cellular mechanisms for differential effects of chronic social isolation stress in males and females. *Molecular Psychiatry*, **27**(7), 3056–3068.

Wolff, M., & Halassa, M. M. (2024). The mediodorsal thalamus in executive control. *Neuron*, **112**(6), 893–908.

Wu, H., Song, Y., Yang, X., Chen, S., Ge, H., Yan, Z., Qi, W., Yuan, Q., Liang, X., Lin, X., & Chen, J. (2023). Functional and structural alterations of dorsal attention network in preclinical and early-stage Alzheimer's disease. *Cell, Nature, and Science Neuroscience & Therapeutics*, **29**(6), 1512–1524.

Xia, Y., Prokop, S., & Giasson, B. I. (2021). "Don't Phos over Tau": Recent developments in clinical biomarkers and therapies targeting tau phosphorylation in Alzheimer's disease and other tauopathies. *Molecular Neurodegeneration*, **16**(1), 37.

Yang, Y. C., Lin, C. H., & Lee, E. H. (2006). Serum- and glucocorticoid-inducible kinase 1 (SGK1) increases neurite formation through microtubule depolymerization by SGK1 and by SGK1 phosphorylation of tau. *Molecular and Cellular Biology*, **26**(22), 8357–8370.

Yoshiyama, Y., Higuchi, M., Zhang, B., Huang, S. M., Iwata, N., Saido, T. C., Maeda, J., Suhara, T., Trojanowski, J. Q., & Lee, V. M. (2007). Synapse loss and microglial activation precede tangles in a P301S tauopathy mouse model. *Neuron*, **53**(3), 337–351.

Zhang, S., Ai, H., Wang, J., Liu, T., Zheng, X., Tian, X., & Bai, W. (2024). Reduced prefrontal-thalamic theta flow during working memory retrieval in APP/PS1 mice. *Journal of Alzheimer's Disease*, **97**(4), 1737–1749.

Zhong, P., Cao, Q., & Yan, Z. (2022). Selective impairment of circuits between prefrontal cortex glutamatergic neurons and basal forebrain cholinergic neurons in a tauopathy mouse model. *Cerebral Cortex*, **32**(24), 5569–5579.

Zhong, P., Cao, Q., & Yan, Z. (2024). Distinct and convergent alterations of entorhinal cortical circuits in two mouse models for Alzheimer's disease and related disorders. *Journal of Alzheimer's Disease*, **98**(3), 1121–1131.

Zhong, P., Qin, L., & Yan, Z. (2020). Dopamine differentially regulates response dynamics of prefrontal cortical principal neurons and interneurons to optogenetic stimulation of inputs from ventral tegmental area. *Cerebral Cortex*, **30**(8), 4402–4409.

Zucker, R. S., & Regehr, W. G. (2002). Short-term synaptic plasticity. *Annual Review of Physiology*, **64**(1), 355–405.

Additional information

Data availability statement

All data are presented and available upon request.

Competing interests

The authors declare no competing interests.

Author contributions

P.Z. performed animal surgery and electrophysiological experiments, analysed data and wrote the draft. T.S. performed animal surgery and immunohistochemistry experiments, and analysed data. P.L. performed some immunohistochemistry experiments. Z.Y. designed experiments, supervised the project and wrote the paper.

Funding

This work was supported by grants from the National Institutes of Health, AG064656 and AG-079797, to Z.Y.

Acknowledgements

We thank Xiaoqing Chen and Mingjun Yu for their excellent technical support.

Keywords

Alzheimer's disease, prefrontal cortex, mediodorsal thalamus, neural circuit, optogenetics, short-term depression, axonal transport, GSK3β, SGK1

Supporting information

Additional supporting information can be found online in the Supporting Information section at the end of the HTML view of the article. Supporting information files available:

Peer Review History